J. Fluid Mech. (1998), *vol.* 371, *pp.* 1–20. Printed in the United Kingdom

The wave modes in ducted swirling flows

By CHRISTOPHER K. W. TAM
AND LAURENT AURIAULT

Department of Mathematics, Florida State University, Tallahassee, FL 32306-4510, USA
email: tam@math.fsu.edu

(Received 8 October 1997 and in revised form 11 April 1998)

The small-amplitude wave modes inside a ducted inviscid compressible swirling flow are investigated. In order to avoid possible mathematical ambiguities arising from the use of an inviscid flow model, the wave modes are cast as the solution of an initial boundary value problem. Two families of propagating waves are found. The acoustic modes are supported by the compressibility effect of the flow. The rotational modes are sustained by the centrifugal force field associated with the mean flow rotation. Two cases, one with a free-vortex swirl and the other with a rigid-body swirl, are investigated in some depth. Numerical results are provided.

1. Introduction

A good understanding of the characteristics of small-amplitude wave modes in a ducted swirling flow is of great importance to turbomachine design and turbomachinery noise prediction. In a uniform inviscid compressible flow, it is well-known (Kovasznay 1953) that the flow supports three types of waves, namely, the acoustic, the vorticity and the entropy waves. In a ducted swirling flow, the situation is much more complicated. There is coupling between compressible and rotational effects so that a simple modal decomposition cannot readily be performed. The analysis of these wave modes has been the subject of a considerable number of investigations in the past.

In a ducted swirling flow, three physical mechanisms are present to sustain wave motions. First is the compressibility of the fluid. This gives rise to the acoustic modes. Second is the centrifugal force field associated with the rotational motion of the mean flow. Spatial variation of this force field is generally sufficient to support axial propagating wave modes. We will refer to these modes as the rotational modes. Finally, shear gradients of the mean velocity profile can, in some instances, support propagating shear waves. For inviscid flow, it is well-known that if an inflection point exists in the velocity profile, the flow will be subjected to Kelvin–Helmholtz instability. However, in typical turbomachines, the mean flow is monotonic and stable. In this work, instability waves generated by velocity gradients will not be considered. Our study will be confined primarily to the acoustic and the rotational wave modes.

The presence of a confining duct wall plays a crucial role in the formation of ducted wave modes. The continuous reflection of disturbances from the wall, when properly phased, leads to constructive reinforcements and cancellations. In this way, a distinctive wave pattern or a wave mode is formed. Because of the need to have precise reinforcements and cancellations, wave speed and frequency that set the timing are crucial to the process. Therefore, the speed of propagation of a duct mode is sensitive to the wave frequency. Thus the duct modes, unlike freely propagating acoustic waves, are intrinsically dispersive.

The study of small-amplitude disturbances in ducted flows began in earnest in the sixties. Tyler & Sofrin (1962) investigated the spinning acoustic modes in a duct with uniform throughflow but no swirl. The effect of non-uniform velocity on the duct modes was investigated by Pridmore-Brown (1958), Mungar & Plumblee (1969), Shankar (1972), Unruh & Eversman (1972), Ko (1973), Swinbanks (1975), Nayfeh, Kaiser & Telionis (1975) and numerous others. For a comprehensive review of the literature on this class of waves, one may consult the article by Eversman (1991). For ducted flows with swirl, the propagation of small-amplitude disturbances has been investigated by Salant (1968), Greitzer & Strand (1978), Kerrebrock (1984, 1987), Yurkovich (1976), Yousefian (1975), Tan & Greitzer (1986). Recently, Wundrow (1994) and Golubev & Atassi (1995, 1997) examined the response of a blade row to incoming disturbances in ducted swirling flows. They followed the work of Goldstein (1978) and Atassi & Gredzinski (1989) in forming a mathematical representation of the input disturbances. Their studies, however, were on the forced response characteristics of the flow and not on its intrinsic wave modes.

Recently, Kousen (1995, 1996) attempted a systematic analysis of the small-amplitude wave modes in a swirling, inviscid, compressible flow in an annulus. He used the standard normal mode approach based on the method of separation of variables. The wave modes were determined by an eigenvalue problem. Kousen computed the eigenvalues and eigenfunctions numerically by the spectral method. His numerical results indicate that there are three families of wave modes. The first family is the Tyler–Sofrin spinning acoustic waves. The second family is related to the swirl of the mean flow that Kousen referred to as the 'nearly convected modes'. The third family forms a continuum of modes. The wavenumber of these waves is such that the convective derivative, $\mathrm{D}/\mathrm{D}t$, of the wave is zero. Kousen called these modes 'purely convected modes'. The existence of the purely convected modes was also suggested in the works of Kerrebrock (1984, 1987). Most recently the problem was investigated by Golubev & Atassi (1997) again using the normal mode approach. Their work focused on the computation of the 'nearly convected modes'. Regarding the families of wave modes supported by the flow, their conclusions are similar to those of Kousen.

The objectives of this investigation are twofold. First, we seek a clarification of the types of wave modes that are sustained by a ducted, inviscid, compressible swirling flow. This will be done by posing the problem as an initial value problem. Secondly, we investigate the intrinsic propagation characteristics of all these wave modes. Knowledge of such characteristics would be helpful to turbomachine loading and noise radiation estimates. They are also essential to the determination of the resolution requirements in any time-domain numerical simulation of these flows.

It is well recognized that if the normal modes of a system are complete then any disturbances can be represented by a simple superposition of the normal modes. In this case, a normal mode analysis of the flow system is sufficient for most purposes. However, for a complex flow system such as that associated with swirling compressible flow inside a duct, the question of completeness cannot be easily ascertained. Under this circumstance, an initial value approach is necessary to provide a complete rigorous analysis of the wave modes. In the literature, there are examples in which ambiguities can arise in the analysis of inviscid flows; e.g. the case of damped Kelvin–Helmholtz waves (see Tam 1975; Tam & Morris 1980). One way to remove such ambiguities is to pose the problem as an initial boundary value problem. As such, time-periodic solutions are time-asymptotic solutions. Since the evolution in time is followed, the solution is complete and most of the ambiguities can be removed by appealing to analytic continuation.

One important result of the present investigation is that, excluding instability wave modes, a ducted inviscid compressible swirling flow will support only two families of waves. They are the acoustic modes and the rotational modes. The acoustic modes are produced by the effect of compressibility while the rotational modes are sustained by the centrifugal force field associated with the mean flow swirl. The so-called purely convected modes do not exist. They are spurious modes produced by an ambiguity in performing a normal mode analysis. In §4, numerical results on the acoustic and rotational modes are reported. The incompressible limit and the no-swirl limit are investigated to show clearly the basic underlying mechanisms responsible for maintaining the two families of wave modes.

2. Initial boundary value formulation

Consider an inviscid compressible non-heat-conducting swirling flow inside an annulus of outer radius R and inner radius σR where σ ($\sigma < 1$) is the hub to tip ratio. Dimensionless variables with R as the length scale, a_t (the sound speed at $r = R$) as the velocity scale, R/a_t as the time scale, ρ_t (the density of the fluid at $r = R$) as the density scale, $\rho_t a_t^2$ as the pressure scale and $\rho_t a_t^2/R$ (force per unit volume) as the body force scale, will be used. The governing equations are the Euler equations. It is easy to show that the most general axisymmetric time-independent flow (denoted by an overbar) in cylindrical coordinates (r, ϕ, x) is,

$$\left.\begin{aligned} \overline{u} = \overline{u}(r), \quad \overline{v} = 0, \quad \overline{w} = \overline{w}(r), \quad \overline{\rho} = \overline{\rho}(r), \\ \overline{p}(r) = -\int_r^1 \frac{\overline{\rho}\,\overline{w}^2}{r}\mathrm{d}r + \overline{p}_0, \end{aligned}\right\} \tag{1}$$

where $\overline{p}_0$ is the pressure at $r = 1$; (u, v, w) are the velocity components in the (x, r, ϕ) directions. In (1) $\overline{u}(r)$, $\overline{w}(r)$ and $\overline{\rho}(r)$ are arbitrary functions of r.

Small-amplitude disturbances superimposed on the above mean flow are governed by the linearized Euler equations. On writing out in full, these equations are

$$\frac{\partial \rho}{\partial t} + \frac{1}{r}\frac{\partial}{\partial r}(\overline{\rho}\, v r) + \frac{\overline{w}}{r}\frac{\partial \rho}{\partial \phi} + \overline{u}\frac{\partial \rho}{\partial x} + \overline{\rho}\left(\frac{1}{r}\frac{\partial w}{\partial \phi} + \frac{\partial u}{\partial x}\right) = 0, \tag{2}$$

$$\overline{\rho}\left[\frac{\partial v}{\partial t} + \overline{u}\frac{\partial v}{\partial x} + \frac{\overline{w}}{r}\frac{\partial v}{\partial \phi} - \frac{2\,\overline{w}\,w}{r}\right] - \rho\frac{\overline{w}^2}{r} = -\frac{\partial p}{\partial r} + F_r, \tag{3}$$

$$\overline{\rho}\left[\frac{\partial w}{\partial t} + \overline{u}\frac{\partial w}{\partial x} + v\frac{\mathrm{d}\,\overline{w}}{\mathrm{d}r} + \frac{\overline{w}}{r}\frac{\partial w}{\partial \phi} + \frac{\overline{w}\,v}{r}\right] = -\frac{1}{r}\frac{\partial p}{\partial \phi} + F_\phi, \tag{4}$$

$$\overline{\rho}\left[\frac{\partial u}{\partial t} + \overline{u}\frac{\partial u}{\partial x} + v\frac{\mathrm{d}\,\overline{u}}{\mathrm{d}r} + \frac{\overline{w}}{r}\frac{\partial u}{\partial \phi}\right] = -\frac{\partial p}{\partial x} + F_x, \tag{5}$$

$$\frac{\partial p}{\partial t} + \overline{u}\frac{\partial p}{\partial x} + \frac{\overline{w}}{r}\frac{\partial p}{\partial \phi} + \frac{\overline{\rho}\,\overline{w}^2}{r}v + \gamma\,\overline{p}\left[\frac{1}{r}\frac{\partial (vr)}{\partial r} + \frac{1}{r}\frac{\partial w}{\partial \phi} + \frac{\partial u}{\partial x}\right] = 0, \tag{6}$$

where F_r, F_ϕ and F_x are body forces, and γ is the ratio of specific heats. These body forces may be regarded as representing the forces imparted to the flow by a rotating blade row. The boundary conditions at the outer and inner walls are

$$r = 1, \qquad v = 0, \tag{7}$$

$$r = \sigma, \qquad v = 0, \tag{8}$$

Equations (2) to (6) and boundary conditions (7) and (8) will be considered as an initial boundary value problem. Since our interest is to find the wave modes supported by the flow and not on the transient behaviour of the system, we will assume zero initial conditions. That is, at $t = 0$

$$u = v = w = \rho = p = 0. \tag{9}$$

Effectively it is the body forces that drive the wave modes of the problem.

The dependence on ϕ can be expanded in a Fourier series. Also we are interested primarily in time-periodic body forces. The period is related to the rotational period of the blade row. Thus, without loss of generality, we will assume that the body forces have the form,

$$\begin{bmatrix} F_r \\ F_\phi \\ F_x \end{bmatrix} = \begin{bmatrix} \widehat{F}_r(r,x) \\ \widehat{F}_\phi(r,x) \\ \widehat{F}_x(r,x) \end{bmatrix} \mathrm{e}^{\mathrm{i}(m\phi - \Omega t)}, \tag{10}$$

where m is an integer and Ω is the forcing angular frequency. It is to be noted that the physical solution is given by the real part of the mathematical solution.

The Fourier–Laplace transform of a function $f(x,t)$ and its inverse $\widetilde{f}(k,\omega)$ are related by

$$\left.\begin{aligned} \widetilde{f}(k,\omega) &= \frac{1}{(2\pi)^2}\int_{-\infty}^{\infty}\int_{0}^{\infty} f(x,t)\mathrm{e}^{-\mathrm{i}(kx-\omega t)}\,\mathrm{d}t\,\mathrm{d}x, \\ f(x,t) &= \int_{-\infty}^{\infty}\int_{\Gamma} \widetilde{f}(k,\omega)\mathrm{e}^{\mathrm{i}(kx-\omega t)}\,\mathrm{d}\omega\,\mathrm{d}k, \end{aligned}\right\} \tag{11}$$

where the inversion contour Γ is taken to be in the upper-half ω-plane parallel to the real ω-axis above all the poles and singularities of the integrand.

It is obvious that the solution of the linear problem has $\mathrm{e}^{\mathrm{i}m\phi}$ dependence. On factoring out $\mathrm{e}^{\mathrm{i}m\phi}$, the Fourier–Laplace transforms of (2) to (6) are

$$-\mathrm{i}\left(\omega - \overline{u}k - \frac{m\overline{w}}{r}\right)\widetilde{\rho} + \overline{\rho}\left[\frac{1}{r}\frac{\mathrm{d}(\widetilde{v}r)}{\mathrm{d}r} + \frac{\mathrm{i}m\widetilde{w}}{r} + \mathrm{i}k\widetilde{u}\right] + \widetilde{v}\frac{\mathrm{d}\overline{\rho}}{\mathrm{d}r} = 0, \tag{12}$$

$$-\mathrm{i}\overline{\rho}\left(\omega - \overline{u}k - \frac{m\overline{w}}{r}\right)\widetilde{v} - \frac{2\overline{\rho}\,\overline{w}}{r}\widetilde{w} - \frac{\overline{w}^2}{r}\widetilde{\rho} = -\frac{\mathrm{d}\widetilde{p}}{\mathrm{d}r} + \frac{\mathrm{i}\widetilde{F}_r}{2\pi(\omega - \Omega)}, \tag{13}$$

$$-\mathrm{i}\overline{\rho}\left(\omega - \overline{u}k - \frac{m\overline{w}}{r}\right)\widetilde{w} + \overline{\rho}\left(\frac{\mathrm{d}\overline{w}}{\mathrm{d}r} + \frac{\overline{w}}{r}\right)\widetilde{v} = \frac{-\mathrm{i}m\widetilde{p}}{r} + \frac{\mathrm{i}\widetilde{F}_\phi}{2\pi(\omega - \Omega)}, \tag{14}$$

$$-\mathrm{i}\overline{\rho}\left(\omega - \overline{u}k - \frac{m\overline{w}}{r}\right)\widetilde{u} + \overline{\rho}\frac{\mathrm{d}\overline{u}}{\mathrm{d}r}\widetilde{v} = -\mathrm{i}k\widetilde{p} + \frac{\mathrm{i}\widetilde{F}_x}{2\pi(\omega - \Omega)}, \tag{15}$$

$$-\mathrm{i}\left(\omega - \overline{u}k - \frac{m\overline{w}}{r}\right)\widetilde{p} + \frac{\overline{\rho}\,\overline{w}^2}{r}\widetilde{v} + \gamma\,\overline{p}\left[\frac{1}{r}\frac{\mathrm{d}(\widetilde{v}r)}{\mathrm{d}r} + \frac{\mathrm{i}m}{r}\widetilde{w} + \mathrm{i}k\widetilde{u}\right] = 0. \tag{16}$$

It is possible, by eliminating all other variables from the above equations, to find a single equation for $\widetilde{p}$. This can be done by first eliminating the square bracketted terms in (12) and (16) to obtain $\widetilde{\rho}$ in terms of $\widetilde{p}$ and $\widetilde{v}$. Thus $\widetilde{\rho}$ in (13) can be replaced by terms involving $\widetilde{p}$ and $\widetilde{v}$. Next, the modified equation (13) can be solved simultaneously with (14) for $\widetilde{v}$ and $\widetilde{w}$ in terms of $\widetilde{p}$. Of use later is the following

relation between $\tilde{v}$ and $\tilde{p}$:

$$\tilde{v} = \frac{-\mathrm{i}}{\Delta}\,\bar{\rho}\,X\left[\left(\frac{\bar{\rho}}{\gamma\,\bar{p}}\,\bar{w}+\frac{2m}{rX}\right)\frac{\bar{w}}{r}\,\tilde{p}-\frac{\mathrm{d}\,\tilde{p}}{\mathrm{d}r}+\frac{\mathrm{i}}{2\pi(\omega-\Omega)}\left(\tilde{F}_r+\frac{2\mathrm{i}\,\bar{w}}{rX}\,\tilde{F}_\phi\right)\right], \tag{17}$$

where

$$X = \left(\omega-\bar{u}\,k-\frac{m\,\bar{w}}{r}\right), \tag{18}$$

$$\Delta = 2\,\bar{\rho}^2\,\frac{\bar{w}}{r}\left(\frac{\mathrm{d}\,\bar{w}}{\mathrm{d}r}+\frac{\bar{w}}{r}\right)-\bar{\rho}^2\,X^2-\frac{\bar{\rho}\,\bar{w}^2}{r}\left(\frac{\bar{\rho}}{\gamma\,\bar{p}}\,\frac{\bar{\rho}\,\bar{w}^2}{r}-\frac{\mathrm{d}\,\bar{\rho}}{\mathrm{d}r}\right). \tag{19}$$

Finally, by substitution into (16) and upon eliminating $\tilde{u}$ by (15), a single second-order differential equation for $\tilde{p}$ is found

$$\begin{aligned}\frac{\mathrm{d}^2\,\tilde{p}}{\mathrm{d}r^2}&+\left[\frac{\Delta}{\bar{\rho}\,X}\frac{\mathrm{d}}{\mathrm{d}r}\left(\frac{\bar{\rho}\,X}{\Delta}\right)+\frac{m}{rX}\left(\frac{\mathrm{d}\,\bar{w}}{\mathrm{d}r}+\frac{\bar{w}}{r}\right)+\frac{k}{X}\frac{\mathrm{d}\,\bar{u}}{\mathrm{d}r}+\frac{1}{r}\right]\frac{\mathrm{d}\,\tilde{p}}{\mathrm{d}r}\\&-\left\{\frac{\Delta}{\bar{\rho}\,X}\frac{\mathrm{d}}{\mathrm{d}r}\left[\frac{\bar{\rho}\,\bar{w}}{r\Delta}\left(\frac{2m}{r}+\frac{\bar{\rho}}{\gamma\,\bar{p}}X\,\bar{w}\right)\right]\right.\\&+\left[\frac{1}{r}+\frac{\bar{\rho}}{\gamma\,\bar{p}}\frac{\bar{w}^2}{r}+\frac{m}{rX}\left(\frac{\mathrm{d}\,\bar{w}}{\mathrm{d}r}+\frac{\bar{w}}{r}\right)+\frac{k}{X}\frac{\mathrm{d}\,\bar{u}}{\mathrm{d}r}\right]\left[\frac{2m\,\bar{w}}{r^2X}+\frac{\bar{\rho}}{\gamma\,\bar{p}}\frac{\bar{w}^2}{r}\right]\\&\left.+\frac{\Delta}{\bar{\rho}^2\,X^2}\left(\frac{\bar{\rho}\,X^2}{\gamma\,\bar{p}}-\frac{m^2}{r^2}-k^2\right)\right\}\tilde{p}=\frac{k\Delta\,\tilde{F}_x}{2\pi\,\bar{\rho}^2\,X^2(\omega-\Omega)}.\end{aligned} \tag{20}$$

In order to keep the non-homogeneous terms on the right-hand side of (20) as simple as possible, we have set $\tilde{F}_r = \tilde{F}_\phi = 0$. In a turbomachine $\tilde{F}_\phi$ is not zero. It is set equal to zero here purely for convenience. It can be shown, however, that the wave propagation characteristics in a ducted environment are independent of the sources, i.e. $\tilde{F}_r$, $\tilde{F}_\phi$ and $\tilde{F}_x$, which produce them. They depend only on the mean flow profiles. For the purpose of investigating the wave mode properties, there is no loss of generality by setting $\tilde{F}_\phi = 0$.

The boundary conditions for $\tilde{p}$ are found by imposing (7) and (8) on (17). This leads to the conditions

$$r = 1, \quad r = \sigma: \quad \left(\frac{\bar{\rho}}{\gamma\,\bar{p}}\,\bar{w}+\frac{2m}{rX}\right)\frac{\bar{w}}{r}\,\tilde{p}-\frac{\mathrm{d}\,\tilde{p}}{\mathrm{d}r}=0. \tag{21}$$

It is useful to note that ω in (20), the Laplace transform variable, is a value on the inversion contour Γ in the complex ω-plane. Since Γ is located in the upper-half ω-plane, ω will have a positive imaginary part. Thus the quantity X cannot be equal to zero (k on the k-inversion contour is real). In other words, equation (20) does not have regular singular points on account of X being zero at some values of r.

The solution of (20) corresponding to arbitrary radial distribution of body force $\tilde{F}_x$ can be found by simple integration over the Green's function of the equation. For the purpose of determining the wave modes supported by the ducted swirling flow, it is sufficient to consider only the Green's function. The Green's function is generated by a highly concentrated body force (the delta function) and would produce all wave modes. In what follows, $\tilde{F}_x$ will be replaced by

$$\tilde{F}_x = \frac{F(k)}{2\pi}\delta\,(r-\bar{r}), \quad \sigma < \bar{r} < 1. \tag{22}$$

Now let $f(r,k,\omega)$ and $g(r,k,\omega)$ be two linearly independent solutions of the homogeneous form of equation (20). The solution of (20) and (22) satisfying boundary condition (21) may be written as a linear combination of f and g following standard procedure of constructing the Green's function of a second order differential equation. It is straightforward to find

$$\tilde{p}(r,k,\omega) = \frac{kF(k)}{2\pi(\omega-\Omega)}\left(\frac{\Delta}{\bar{\rho}^2 X^2}\right)_{r=\bar{r}} \times \frac{[f(r_>,k,\omega)+c_1 g(r_>,k,\omega)][f(r_<,k,\omega)+c_\sigma g(r_<,k,\omega)]}{(c_1-c_\sigma)[f(\bar{r},k,\omega)g'(\bar{r},k,\omega)-f'(\bar{r},k,\omega)g(\bar{r},k,\omega)]}, \tag{23}$$

where $r_>$ ($r_<$) is the greater (lesser) of r and $\bar{r}$, $g' = \mathrm{d}g/\mathrm{d}r$, $f' = \mathrm{d}f/\mathrm{d}r$ and

$$c_1 = \frac{\left[\dfrac{\mathrm{d}f}{\mathrm{d}r} - \left(\dfrac{\bar{\rho}}{\gamma\,\bar{p}}\,\bar{w} + \dfrac{2m}{rX}\right)\dfrac{\bar{w}}{r}f\right]_{r=1}}{\left[\left(\dfrac{\bar{\rho}}{\gamma\,\bar{p}}\,\bar{w} + \dfrac{2m}{rX}\right)\dfrac{\bar{w}}{r}g - \dfrac{\mathrm{d}g}{\mathrm{d}r}\right]_{r=1}}, \tag{24}$$

$$c_\sigma = \frac{\left[\dfrac{\mathrm{d}f}{\mathrm{d}r} - \left(\dfrac{\bar{\rho}}{\gamma\,\bar{p}}\,\bar{w} + \dfrac{2m}{rX}\right)\dfrac{\bar{w}}{r}f\right]_{r=\sigma}}{\left[\left(\dfrac{\bar{\rho}}{\gamma\,\bar{p}}\,\bar{w} + \dfrac{2m}{rX}\right)\dfrac{\bar{w}}{r}g - \dfrac{\mathrm{d}g}{\mathrm{d}r}\right]_{r=\sigma}}. \tag{25}$$

The solution in physical space and time can now be found by inverting the Fourier–Laplace transforms. By means of (23), we have,

$$p(r,x,t) = \frac{1}{2\pi}\int_\Gamma\int_{-\infty}^{\infty}\frac{kF(k)}{(\omega-\Omega)}\left(\frac{\Delta}{\bar{\rho}^2 X^2}\right)_{r=\bar{r}} \times \frac{[f(r_>,k,\omega)+c_1 g(r_>,k,\omega)][f(r_<,k,\omega)+c_\sigma g(r_<,k,\omega)]\mathrm{e}^{\mathrm{i}(kx-\omega t)}}{(c_1-c_\sigma)[f(\bar{r},k,\omega)g'(\bar{r},k,\omega)-f'(\bar{r},k,\omega)g(\bar{r},k,\omega)]}\mathrm{d}k\,\mathrm{d}\omega. \tag{26}$$

Equation (26) has a pole on the real ω-axis at $\omega = \Omega$ (the forcing frequency). Of interest to us are the neutral propagating wave modes. These modes come from the poles of the integrand lying on the real k-axis in the complex k-plane. The factor $[f(\bar{r},k,\omega)g'(\bar{r},k,\omega)-f'(\bar{r},k,\omega)g(\bar{r},k,\omega)]$ in the denominator of the integrand of (26) is the Wronskian of f and g. By assumption, f and g are linearly independent solutions for $\sigma \leqslant \bar{r} \leqslant 1$. The Wronskian cannot be equal to zero. Therefore, the poles of the integrand come from the zeros of $(c_1 - c_\sigma)$. That is

$$D(k,\omega) \equiv \left[\left(\frac{\bar{\rho}}{\gamma\,\bar{p}}\,\bar{w} + \frac{2m}{rX}\right)\frac{\bar{w}}{r}f - \frac{\mathrm{d}f}{\mathrm{d}r}\right]_{r=1}\left[\left(\frac{\bar{\rho}}{\gamma\,\bar{p}}\,\bar{w} + \frac{2m}{rX}\right)\frac{\bar{w}}{r}g - \frac{\mathrm{d}g}{\mathrm{d}r}\right]_{r=\sigma} - \left[\left(\frac{\bar{\rho}}{\gamma\,\bar{p}}\,\bar{w} + \frac{2m}{rX}\right)\frac{\bar{w}}{r}f - \frac{\mathrm{d}f}{\mathrm{d}r}\right]_{r=\sigma}\left[\left(\frac{\bar{\rho}}{\gamma\,\bar{p}}\,\bar{w} + \frac{2m}{rX}\right)\frac{\bar{w}}{r}g - \frac{\mathrm{d}g}{\mathrm{d}r}\right]_{r=1} = 0. \tag{27}$$

Equation (27) is the dispersion relation. Since Γ is in the upper-half ω-plane, we can deform the contour as shown in figure 1 to pick up the pole at $\omega = \Omega$. During the contour deformation process, some zeros of $D(k,\omega)$ in the k-plane move to the real k-axis. Some zeros may even cross over from the upper-half to the lower-half k-plane and vice versa. The k-inversion contour must be deformed as shown in figure 2 to avoid crossing by the poles. This is necessary to maintain analytic continuation. This

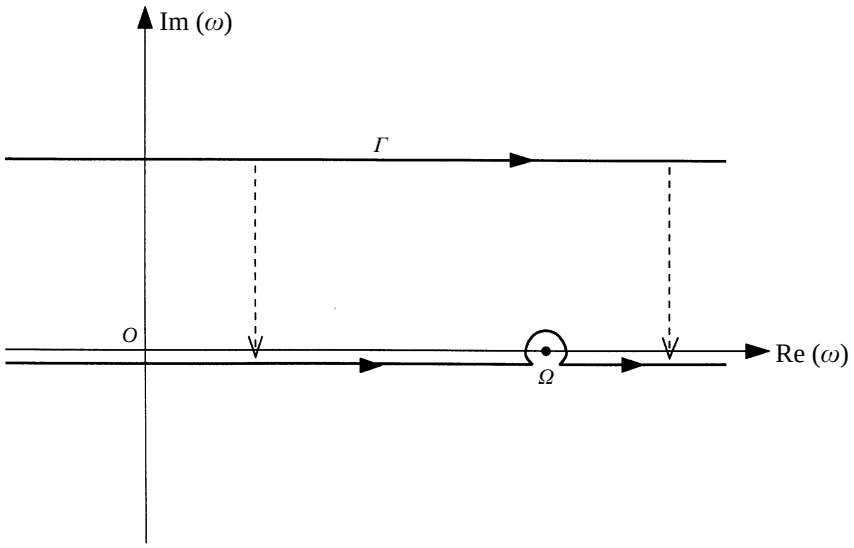

FIGURE 1. Deformation of the inversion contour Γ to the real ω-axis to pick up the pole at Ω.

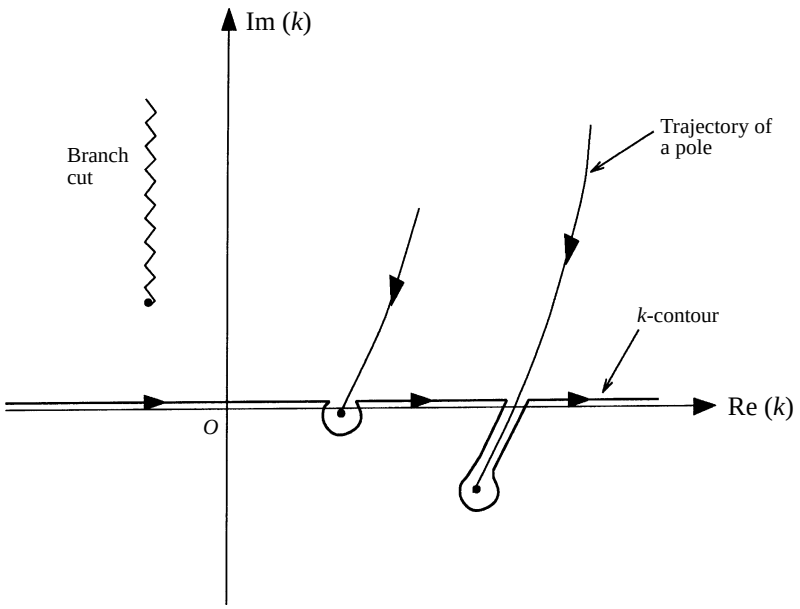

FIGURE 2. Deformation of the k-inversion contour in the k-plane for poles coming from the upper-half plane during the deforming of the Γ-contour in the ω-plane; $x > 0$.

contour deformation process has been described in detail and used by Tam & Hu (1989*a*,*b*). The poles that cross the real k-axis will give rise to spatially amplifying waves. The poles that reach the real k-axis will give rise to undamped propagating wave modes. For $x > 0$, the propagating modes are given by the residues of the poles that reach the real k-axis starting from the upper-half plane. For $x < 0$, the propagating modes are given by the residues of the poles that reach the real k-axis starting from the lower-half plane. For the purpose of determining the type of neutral propagating modes of the flow, we have, by evaluating the contributions from the

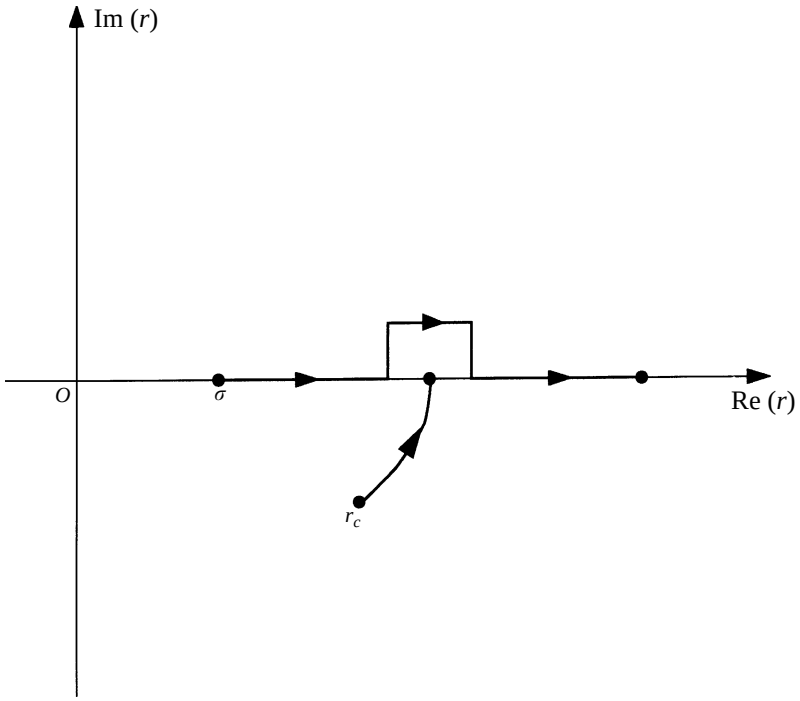

FIGURE 3. Deformation of the r-integration contour in the complex r-plane when r_c approches the real axis.

pole at $\omega = \Omega$ and the poles in the k-plane,

$$p(r,x,t) = \begin{cases} 2\pi \sum_{j=1}^{J} \left[\left(\dfrac{\Delta}{\bar{\rho}^2 X^2} \right)_{r=\bar{r}} kF(k) \right. \\ \quad \left. \times \dfrac{[f(r_>,k,\omega) + c_1 g(r_>,k,\omega)][f(r_<,k,\omega) + c_\sigma g(r_<,k,\omega)]\mathrm{e}^{\mathrm{i}(kx-\Omega t)}}{[f(\bar{r},k,\omega)g'(\bar{r},k,\omega) - f'(\bar{r},k,\omega)g(\bar{r},k,\omega)]\partial/\partial k(c_1 - c_\sigma)} \right]_{\omega=\Omega,k=k_j} \\ \quad + \ldots; \quad x > 0, \\ -2\pi \sum_{i=1}^{I} \left[\left(\dfrac{\Delta}{\bar{\rho}^2 X^2} \right)_{r=\bar{r}} kF(k) \right. \\ \quad \left. \times \dfrac{[f(r_>,k,\omega) + c_1 g(r_>,k,\omega)][f(r_<,k,\omega) + c_\sigma g(r_<,k,\omega)]\mathrm{e}^{\mathrm{i}(kx-\Omega t)}}{[f(\bar{r},k,\omega)g'(\bar{r},k,\omega) - f'(\bar{r},k,\omega)g(\bar{r},k,\omega)]\partial/\partial k(c_1 - c_\sigma)} \right]_{\omega=\Omega,k=k_i} \\ \quad + \ldots; \quad x < 0, \end{cases} \tag{28}$$

where k_j $(j = 1,2,\ldots,J)$ are the zeros of $D(k,\omega)$ that move from the upper-half k-plane to the real k-axis during the contour deformation process and k_i $(i = 1,2,\ldots,I)$ are the corresponding zeros that move to the real axis from the lower-half k-plane.

It is observed that for ω and k both real, $X = (\omega - k\,\bar{u} - m\,\bar{w}/r)$ may become zero at some value of r, say $r = r_c$. When this happens (20) would have a regular singular point at $r = r_c$. Mathematically, such a solution is not the correct analytical continuation of the physical solution. The correct analytical continuation solution is obtained by deforming the integration contour in the complex r-plane as shown

in figure 3. This procedure has been discussed and used by Tam (1975) and Tam & Morris (1980). By deforming the contour in the r-plane to avoid crossing the critical point r_c, X will remain unequal to zero. In this way, analytic continuation is maintained.

Now the coefficients of equation (20) are real as long as ω and k are real and X never becomes zero for $\sigma \leqslant r \leqslant 1$. It follows that the two linearly independent homogeneous solutions f and g are real. Under this condition $D(k, \omega)$ is real and hence some of the roots of $D(k, \Omega) = 0$ are real. That is, the flow supports neutral propagating wave modes. On the other hand, for real k and ω if X becomes zero for $\sigma \leqslant r \leqslant 1$, the r-integration must be carried out on the deformed contour. The result is that f and g are complex. Hence $D(k, \Omega)$ is also complex. In this case the roots of $D(k, \Omega) = 0$ would be complex, so that there is no neutral propagating mode. This means that the so-called 'purely convected modes' cannot exist.

3. Free-vortex swirl

In the past, a number of investigators (e.g. Kerrebrock 1984, 1987; Wundrow 1994; Golebev & Atassi 1995) used a free-vortex swirl superimposed on a uniform axial throughflow as a mean flow model for the study of small amplitude wave modes inside an annulus. Mathematically, the mean flow is taken to be,

$$\overline{u} = M, \quad \overline{v} = 0, \quad \overline{w} = \frac{\Gamma}{r}, \quad \overline{\rho} = 1, \quad \overline{p} = \frac{\Gamma^2}{2}\left(1 - \frac{1}{r^2}\right) + \frac{1}{\gamma}, \tag{29}$$

where M is the axial Mach number and Γ is the circulation. Recently, this flow was studied more carefully by Kousen (1995, 1996). He carried out extensive computation of the dispersion relation of the various types of wave modes supported by the free-vortex swirl using the spectral method. He reported the finding of a continuum of 'purely convected' modes with wavenumber given by $X = (\Omega - Mk - m\Gamma/r^2) = 0$ for $\sigma \leqslant r \leqslant 1$. The possible existence of these purely convected modes was elaborated earlier by Kerrebrock (1984, 1987).

There is currently a rich literature on the stability of rotating flows. For inviscid fluid, Rayleigh (1916) (see Lin 1967, Chapter 4; Chandrasekhar 1961, Chapter 7) established that the necessary and sufficient condition for stability is

$$\frac{\mathrm{d}}{\mathrm{d}r}(\overline{w}\, r)^2 > 0. \tag{30}$$

It is easy to verify that for the free-vortex swirl, this stability criterion is violated. Thus the flow is basically unstable and the finding of an unstable mode should not be at all unexpected.

In this section, we will report our numerical results on the wave modes of the free-vortex swirl and compare them with those of the previous investigators. According to the analysis of the previous section, the wavenumbers of the wave modes of the flow are given by the roots of

$$D(k, \omega) = 0, \tag{31}$$

where D is the dispersion function of (27). To calculate D, two linearly independent solutions f and g of the homogeneous equation (20) must first be found. In this work, the solutions are obtained by direct numerical integration of the second-order differential equation using the Runge–Kutta scheme. However, it is noticed that for large k the equation is stiff. To ensure that the two numerical solutions are, indeed,

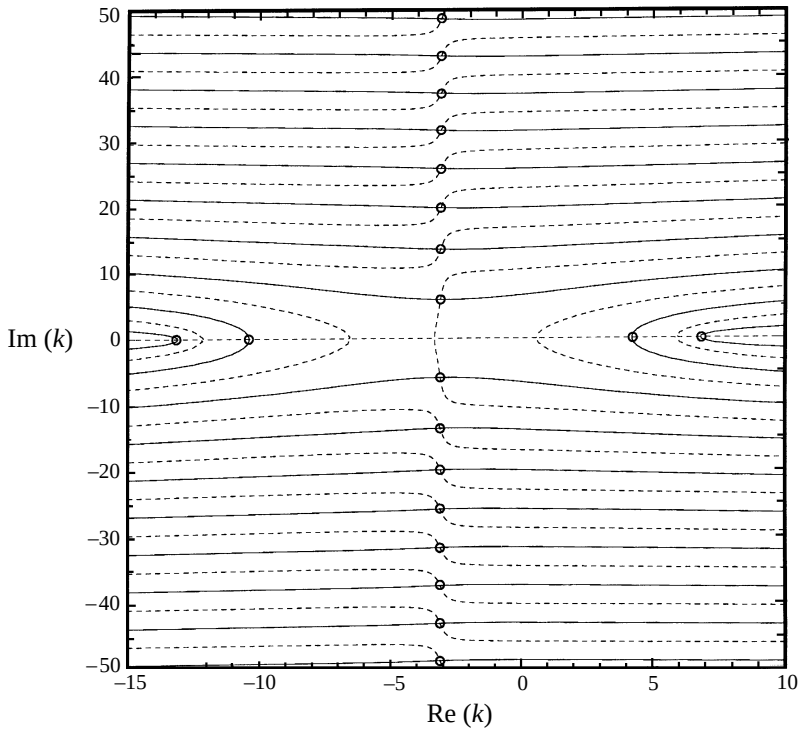

FIGURE 4. Wavenumbers of the acoustic modes in a free vortex swirl flow. ————, $\mathrm{Re}(D) = 0$; – – – – –, $\mathrm{Im}(D) = 0$. $M = 0.3$, $m = 2$, $\Omega = 10.0$, $\Gamma = 0.2$, $\sigma = 0.4$.

linearly independent, the method of orthonormalization (see Scott & Watts 1977) is followed in the integration process.

To locate the roots of $D(k, \Omega)$ in the complex k-plane, the grid search method of Tam & Hu (1989*a*,*b*) is employed. In this method, the region in the k-plane where the zeros of D are to be found is first divided into a fine grid. The values of D are then calculated at each of the grid points. Next, the curves $\mathrm{Re}(D) = 0$ and $\mathrm{Im}(D) = 0$ are determined by a two-dimensional interpolation programme using the values of D on the grid. The intersection points of these two sets of curves automatically give the roots of D. The grid search method is accurate and efficient. When higher accuracy is desired, a Newton iteration refinement is applied using the roots of the grid search as starting points.

We concentrate our numerical effort on the case $M = 0.3$, $\Gamma = 0.2$, $m = 2$, $\sigma = 0.4$, $\Omega = 10.0$ of the free-vortex swirl flow. This is the same flow as studied by Kousen (1996). There are two types of waves. The wave modes that are of acoustic origin have wavenumbers in the range $-15.0 < k < 10.0$. Figure 4 shows the wavenumbers of these modes in the complex k-planes located by the grid search method. The roots of D lying off the real k-axis are damped waves. There are two acoustic wave modes with real positive k-values and two acoustic wave modes with real negative k-values. The former are waves propagating in the positive x-direction while the latter are waves propagating in the negative x-direction. In Kousen's paper, three positive and three negative real k-values are found. However, two of each of the three k-values are very close to each other. We suspect that they are the same mode but are split off by

the numerical algorithm used. Except for this difference, the numerical values of the present finding are in good agreement with those of Kousen (1996).

If purely convected modes exist for the free-vortex swirl flow under consideration, their wavenumbers should lie along the real k-axis in the range of $25 \leqslant k \leqslant 32$. If we perform a grid search over the rectangle $25 \leqslant \mathrm{Re}(k) \leqslant 32$ and $-2.0 \leqslant \mathrm{Im}(k) \leqslant 0.5$, we find no zero of $D(k, \omega)$ on the real k-axis. Instead, our search locates a spatially amplifying (unstable) wave mode at $k = (26.18 - 0.238\mathrm{i})$ propagating to the positive x-direction. In order to show that this is, indeed, a spatially amplifying wave mode, the wavenumber of this mode is first located in the complex k-plane with ω set equal to $(10.0 + 0.2\mathrm{i})$. This corresponds to Γ lying in the upper-half ω-plane. This is shown in figure 5(*a*). The imaginary part of ω is subsequently reduced and the movement of the wavenumber of this mode is tracked. At $\omega = (10.0 + 0.1\mathrm{i})$, the location of the wavenumber is at the real k-axis. Finally, as the imaginary part of ω is further reduced, the wavenumber crosses the real k-axis into the lower-half k-plane and reaches the value $(26.18 - 0.239\mathrm{i})$ when $\mathrm{Im}(\Omega)$ becomes zero, figure 5(*b*). Thus this mode that originates in the upper-half k-plane is truly a spatially amplifying wave created by the instability of the free-vortex swirl. Figure 6 shows the spatial distribution of the real and imaginary part of the pressure eigenfunction associated with the spatially amplifying wave. It is evident that the pressure fluctuations are concentrated mainly near the hub of the annulus. This is, perhaps, not too surprising for this is where the swirl is the strongest.

4. The acoustic and the rotational modes

Inside a ducted inviscid compressible swirling flow, there are basically two types of propagating wave modes, assuming that there are no instability waves. They are the acoustic modes and the rotational modes. To illustrate the main features of the acoustic and the rotational modes, we will consider a mean flow characterized by a rigid-body swirl. That is,

$$\overline{u} = M, \quad \overline{v} = 0, \quad \overline{w} = \overline{\Omega}\, r, \quad \overline{\rho} = 1, \quad \overline{p} = \frac{1}{\gamma} - \frac{\overline{\Omega}^2}{2}(1 - r^2). \tag{32}$$

The rigid-body swirl model is a good representation of the mean flow in turbomachines. It has been used by Salant (1968), Kerrebrock (1984, 1987), Golebev & Atassi (1995) and Kousen (1995, 1996) in their works on small amplitude wave modes in ducted swirling flows.

In order to show unambiguously that acoustic modes are sustained by compressibility effects while rotational modes are maintained by mean flow swirl, we will focus on two special limits. First, we will consider the incompressible limit. In this case, there cannot be any acoustic modes. All the wave modes of the flow system are rotational modes. Second, we will consider the no-swirl limit, i.e. $\overline{\Omega} \to 0$. In this case, the flow has only acoustic modes.

4.1. *The incompressible limit*

In the incompressible limit, with (32) as the mean flow, (20) becomes

$$\frac{\mathrm{d}^2 \widetilde{p}}{\mathrm{d}r^2} + \frac{1}{r}\frac{\mathrm{d}\widetilde{p}}{\mathrm{d}r} + \left[k^2 \frac{(4\,\overline{\Omega}^2 - X^2)}{X^2} - \frac{m^2}{r^2}\right] \widetilde{p} = \frac{\Delta}{2\pi(\omega - \Omega)X^2} kF(k)\delta(r - \overline{r}), \tag{33}$$

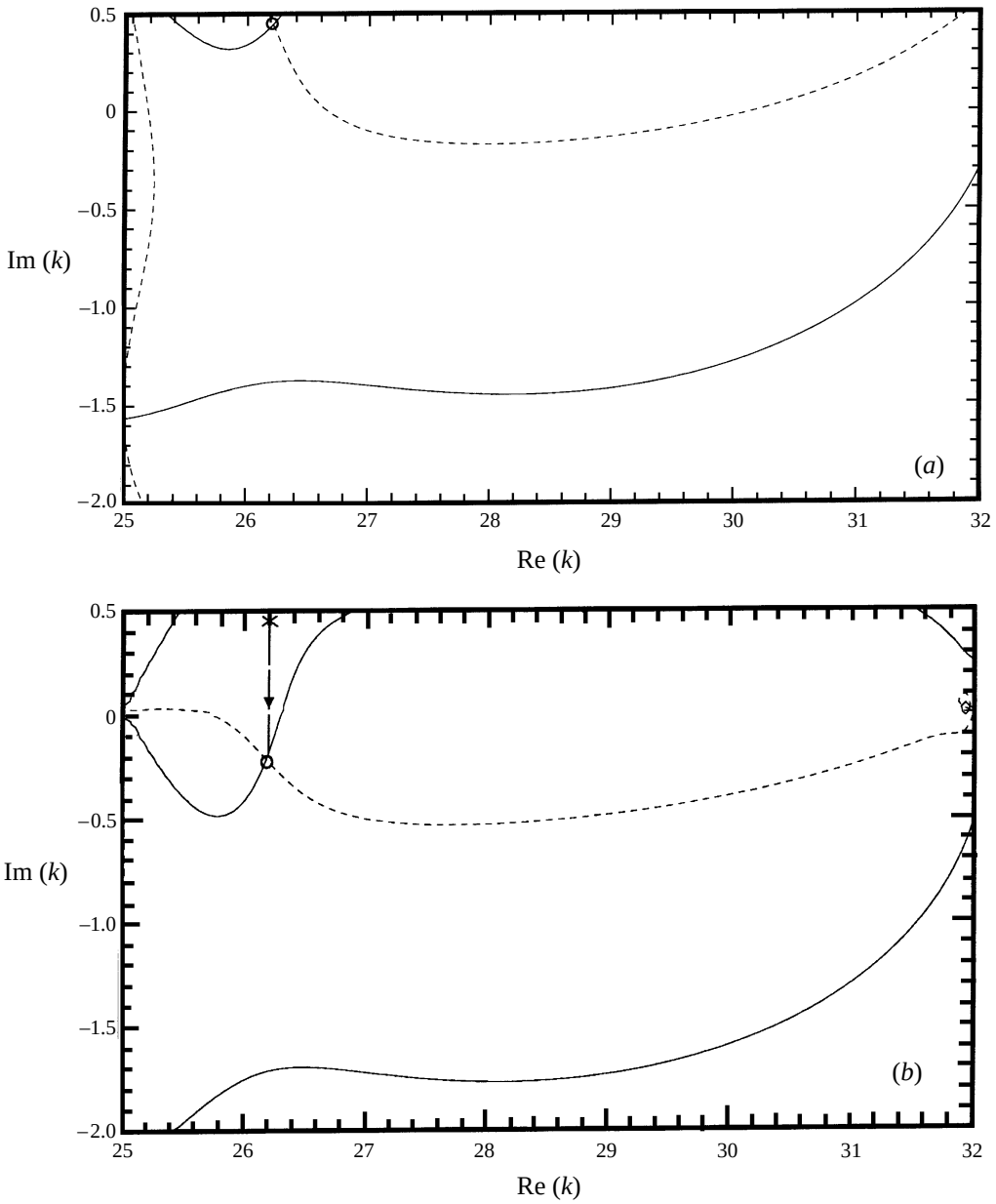

FIGURE 5. (*a*) The instability wavenumber in a free vortex swirl flow. ————, $\mathrm{Re}(D) = 0$; – – – – –, $\mathrm{Im}(D) = 0$. $M = 0.3$, $m = 2$, $\Gamma = 0.2$, $\sigma = 0.4$, $\Omega = 10.0 + 0.2\mathrm{i}$ (*b*) Same as (*a*) except $\Omega = 10.0$; ×——→—— trajectory of unstable pole.

where

$$X = \omega - Mk - m\overline{\Omega}, \qquad \Delta = 4\overline{\Omega}^2 - X^2. \tag{34}$$

The two linearly independent homogeneous solutions of (33) are the Bessel and Neumann functions of order m, i.e. $J_m(k(4\overline{\Omega}^2 - X^2)^{1/2} r/X)$ and $Y_m(k(4\overline{\Omega}^2 - X^2)^{1/2} r/X)$. The branch cuts of the square root function $(4\overline{\Omega}^2 - X^2)^{1/2}$ in the arguments of these

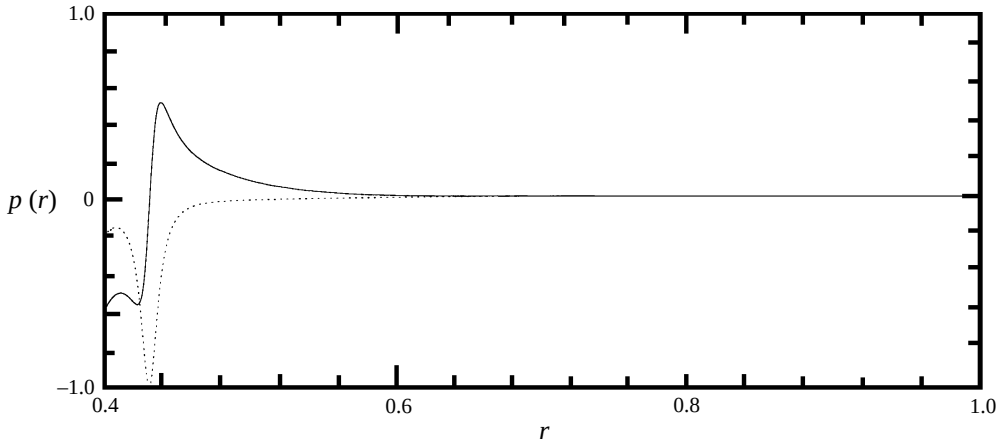

FIGURE 6. Pressure eigenfunction of the free vortex swirl instability wave: ————, real part; · · · · · · · · ·, imaginary part. $M = 0.3$, $m = 2$, $\Omega = 10.0$, $\Gamma = 0.2$ $\sigma = 0.4$.

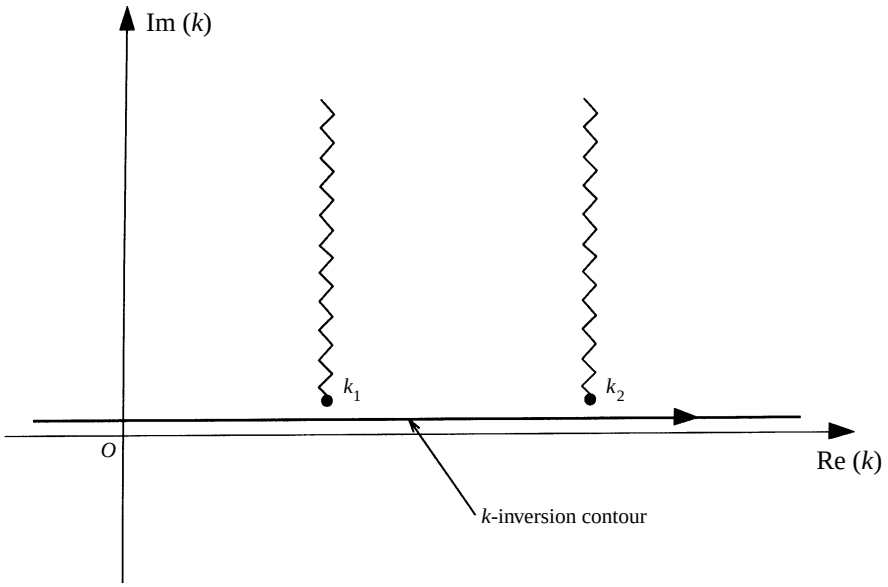

FIGURE 7. The branch cuts of the function $(4\overline{\Omega}^2 - X^2)^{1/2}$ in the k-plane.

functions need to be clearly defined in the k-plane. Here we will let

$$(4\overline{\Omega}^2 - X^2)^{1/2} = \mathrm{e}^{3\pi \mathrm{i}/2}(k - k_1)^{1/2}(k - k_2)^{1/2}M. \tag{35}$$

The branch points k_1 and k_1 are

$$k_1 = \frac{\omega + (2 - m)\,\overline{\Omega}}{M}, \quad k_2 = \frac{\omega - (2 + m)\,\overline{\Omega}}{M}. \tag{36}$$

Figure 7 shows the branch cuts of this function in the k-plane. The behaviour of the Bessel and Neumann functions for real k depends on whether $(4\overline{\Omega}^2 - X^2)^{1/2}$ is real or purely imaginary. When this function is real both the Bessel and Neumann functions are real. Further, real Bessel and Neumann functions are oscillatory with many zeros. The existence of these zeros makes it possible for the solution (eigenfunction) to satisfy

the homogeneous boundary conditions at $r = 1$ and $r = \sigma$. Therefore, propagating modes are possible for

$$k_2 < k < k_1. \tag{37}$$

Outside this range of k (real k), the solutions are the modified Bessel and Hankel functions. These are monotonic functions. Hence they cannot satisfy the homogeneous boundary conditions at the hub and the tip. Thus there will not be propagating wave modes with wavenumber k lying outside the range of (37).

For incompressible rigid-body swirl flow, dispersion relation (27) simplifies to

$$\left[\kappa J'_m(\kappa\sigma) - \frac{2m\overline{\Omega}}{X} J_m(\kappa\sigma)\right]\left[\kappa Y'_m(\kappa) - \frac{2m\overline{\Omega}}{X} Y_m(\kappa)\right] - \left[\kappa J'_m(\kappa) - \frac{2m\overline{\Omega}}{X} J_m(\kappa)\right]\left[\kappa Y'_m(\kappa\sigma) - \frac{2m\overline{\Omega}}{X} Y_m(\kappa\sigma)\right] = 0, \tag{38}$$

where

$$\kappa \equiv \kappa(k) = \frac{kM}{X} e^{3\pi i/2}(k - k_1)^{1/2}(k - k_2)^{1/2}. \tag{39}$$

The wavenumbers of the rotational modes are given by the roots of (38) in the range $k_2 < k < k_1$. From (28), the pressure field associated with a rotational mode of wavenumber k_n (including the dependence on ϕ) may be written out explicitly as,

$$p(r, \phi, x, t) = 2\pi \frac{k_n \Delta_n F(k_n)}{\kappa_n X_n} \times \frac{\left[J_m(\kappa_n r_>) - \dfrac{\kappa_n J'_m(\kappa_n) - (2m\overline{\Omega}/X_n)J_m(\kappa_n)}{\kappa_n Y'_m(\kappa_n) - (2m\overline{\Omega}/X_n)Y_m(\kappa_n)} Y_m(\kappa_n r_>)\right]}{\left[J_m(\kappa_n \bar{r}) Y'_m(\kappa_n \bar{r}) - J'_m(\kappa_n \bar{r}) Y_m(\kappa_n \bar{r})\right]} \times \left.\frac{\left[J_m(\kappa_n r_<) - \dfrac{\kappa_n J'_m(\kappa_n\sigma) - (2m\overline{\Omega}/X_n)J_m(\kappa_n\sigma)}{\kappa_n Y'_m(\kappa_n\sigma) - (2m\overline{\Omega}/X_n)Y_m(\kappa_n\sigma)} Y_m(\kappa_n r_<)\right]}{\dfrac{d}{dk_n}\left[\dfrac{\kappa_n J'_m(\kappa_n\sigma) - (2m\overline{\Omega}/x_n)J_m(\kappa_n\sigma)}{\kappa_n Y'_m(\kappa_n\sigma) - (2m\overline{\Omega}/X_n)Y_m(\kappa_n\sigma)} - \dfrac{\kappa_n J'_m(\kappa_n) - (2m\overline{\Omega}/x_n)J_m(\kappa_n)}{\kappa_n Y'_m(\kappa_n) - (2m\overline{\Omega}/X_n)Y_m(\kappa_n)}\right]}\right|_{\omega=\Omega} \times e^{i(k_n x + m\phi - \Omega t)}, \quad x > 0, \tag{40}$$

where $r_>$ ($r_<$) is the larger (smaller) of r and $\bar{r}$, κ_n is $\kappa(k_n)$ given by (39), X_n and Δ_n are given by (34) with k replaced by k_n and ω by Ω, the forcing frequency. It is straightforward to write down an expression similar to (40) valid for $x < 0$ (upstream propagating waves).

Figure 8 shows the wavenumbers of the rotational modes in an incompressible rigid-body swirl flow for $M = 0.3$, $\overline{\Omega} = 0.5$, $m = 2$, $\Omega = 10.0$ and $\sigma = 0.4$. They are the roots of (38) and lie in the range $26.7 < k < 33.3$. In the incompressible limit, the rotational modes are the only propagating modes of the flow. If the compressibility effect is included, the wavenumbers of these modes are slightly modified. Figure 9 shows the wavenumbers of the rotational as well as the acoustic modes in the k-plane. They are in good agreement with the calculations of Kousen (1996), the exception being that Kousen included a band of spurious purely convected modes. Figure 10 is a portion of the magnified k-plane showing the effect of compressibility on the wavenumbers of the rotational modes. For the wave modes shown, compressibility effects reduce the wave speed and the wavelength. The reduction is, however, very small.

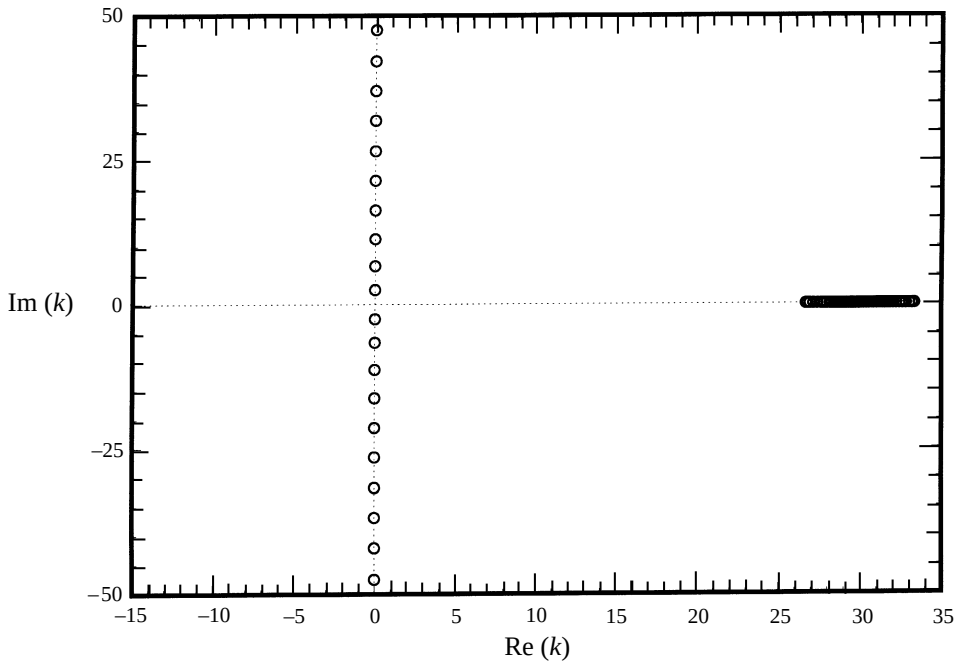

FIGURE 8. Wavenumbers of the rotational modes in an incompressible inviscid rigid-body swirl flow. $M = 0.3$, $\overline{\Omega} = 0.5$, $m = 2$, $\Omega = 10.0$, $\sigma = 0.4$.

4.2. *The no-swirl limit*

If swirl is dropped from the mean flow of (32) the non-homogeneous equation (20) and boundary condition (21) become

$$\frac{\mathrm{d}^2\widetilde{p}}{\mathrm{d}r^2} + \frac{1}{r}\frac{\mathrm{d}\widetilde{p}}{\mathrm{d}r} + \left[(\omega - Mk)^2 - k^2 - \frac{m^2}{r^2}\right]\widetilde{p} = \frac{-k}{2\pi(\omega - \Omega)}\widetilde{F}_x(r,k). \tag{41}$$

At $r = 1$, σ

$$\frac{\mathrm{d}\widetilde{p}}{\mathrm{d}r} = 0. \tag{42}$$

It is easy to show that the homogeneous problem of (41) and (42) forms a Sturm–Liouville eigenvalue problem. The Sturm–Liouville theorem assures that the eigenfunctions form a complete orthogonal set. The eigenfunctions, $y_{mn}(r)$, are a linear combination of the mth-order Bessel and Neumann function

$$y_{mn}(r) = \left[J_m(\lambda_{mn}r) - \frac{J'_m(\lambda_{mn})}{Y'_m(\lambda_{mn})}Y_m(\lambda_{mn}r)\right], \tag{43}$$

where λ_{mn} $(n = 1, 2, \ldots)$ are the eigenvalues. The eigenvalues are the roots of

$$J'_m(\lambda_{mn}\sigma)Y'_m(\lambda_{mn}) - J'_m(\lambda_{mn})Y'_m(\lambda_{mn}\sigma) = 0. \tag{44}$$

The eigenfunctions are complete so the solution $\widetilde{p}$ of (41) can be expanded in a series of the eigenfunctions, i.e.

$$\widetilde{p}(r,k,\omega) = \sum_{n=1}^{\infty} A_n y_{mn}(r). \tag{45}$$

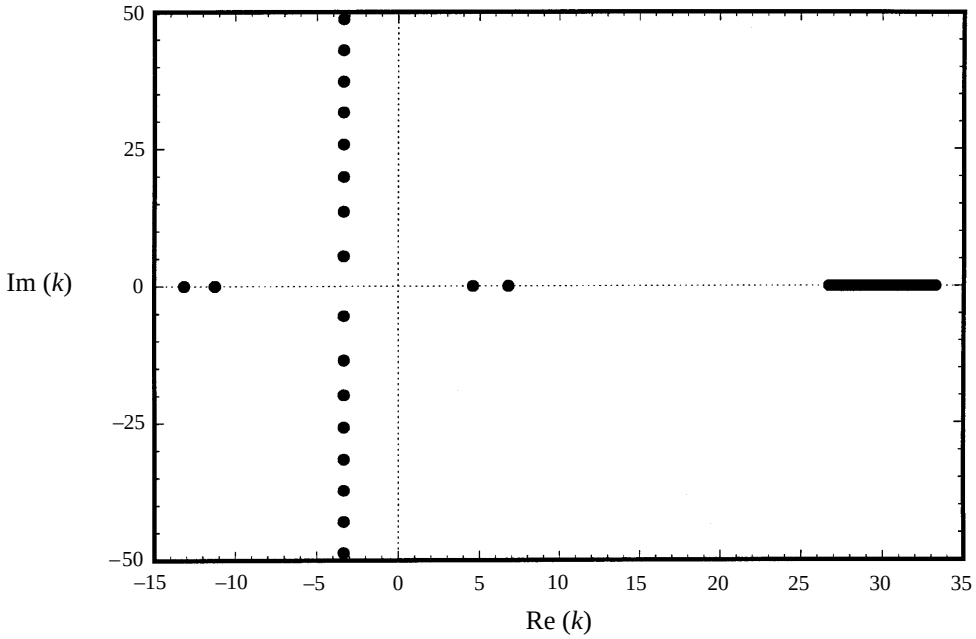

FIGURE 9. Wavenumbers of the rotational and acoustic modes in a compressible inviscid rigid-body swirl flow. $M = 0.3$, $\overline{\Omega} = 0.5$, $m = 2$, $\Omega = 10.0$, $\sigma = 0.4$.

The coefficient A_n can be readily found by the substitution of (45) into (41) and the use of the orthogonality property of the eigenfunctions. This yields

$$A_n = \frac{-\dfrac{2k\lambda_{mn}^2}{\omega - \Omega}\displaystyle\int_\sigma^1 \widetilde{F}_x(k,r)y_{mn}(r)r\,\mathrm{d}r}{[(\lambda_{mn}^2 - m^2)\,y_{mn}^2(1) - (\lambda_{mn}^2\sigma^2 - m^2)\,y_{mn}^2(\sigma)][(\omega - Mk)^2 - k^2 - \lambda_{mn}^2]}. \tag{46}$$

The pressure field in space and time associated with the acoustic modes excited by the body force F_x may be found by performing the Fourier–Laplace inverse transform on (45). It is a simple matter to find, after some algebra,

$$p(r,\phi,x,t) = \begin{cases} \displaystyle\sum_n \frac{4\pi^2\lambda_{mn}^2 k_n^+ F_n(k_n^+)y_{mn}(r)\mathrm{e}^{\mathrm{i}(k_n^+ x + m\phi - \Omega t)}}{[(\lambda_{mn}^2 - m^2)y_{mn}^2(1) - (\lambda_{mn}^2\sigma^2 - m^2)y_{mn}^2(\sigma)][\Omega M + (1-M^2)k_n^+]}, & x > 0 \\ \displaystyle\sum_n \frac{-4\pi^2\lambda_{mn}^2 k_n^- F_n(k_n^-)y_{mn}(r)\mathrm{e}^{\mathrm{i}(k_n^- x + m\phi - \Omega t)}}{[(\lambda_{mn}^2 - m^2)y_{mn}^2(1) - (\lambda_{mn}^2\sigma^2 - m^2)y_{mn}^2(\sigma)][\Omega M + (1-M^2)k_n^-]}, & x < 0 \end{cases} \tag{47}$$

where

$$k_n^\pm = \frac{-\Omega M \pm [\Omega^2 - (1-M^2)\lambda_{mn}^2]^{1/2}}{1-M^2}, \tag{48}$$

$$F_n(k) = \int_\sigma^1 \widetilde{F}_x(k,r)y_{mn}(r)r\,\mathrm{d}r. \tag{49}$$

In (47) the summation needs to be carried out for values of n for which $k_n^\pm$ are real.

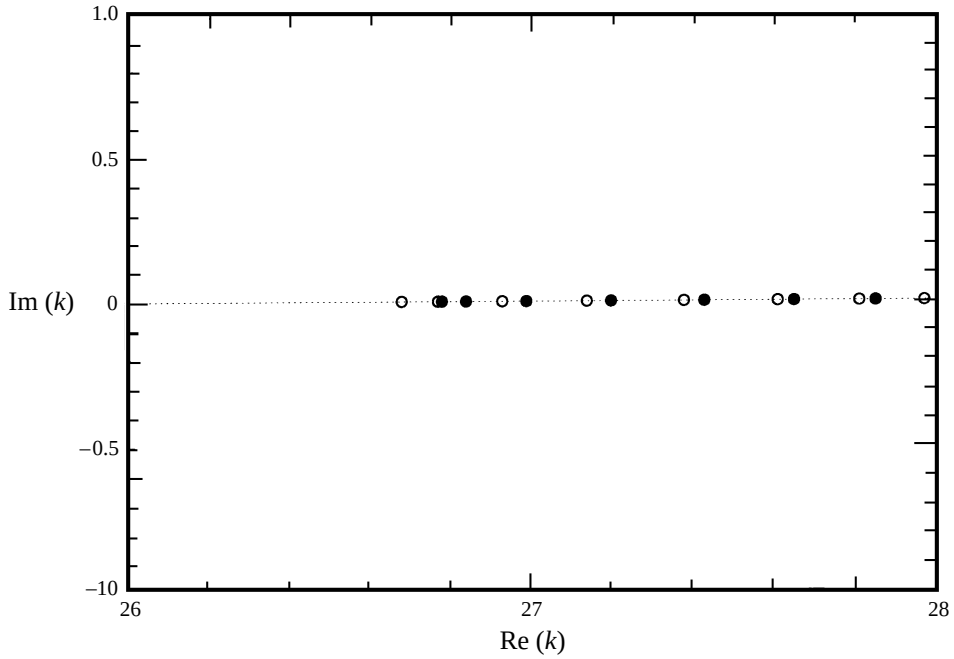

FIGURE 10. The magnified k-plane showing the effect of compressibility on the rotational modes in a rigid-body swirl flow: o, incompressible; •, compressible.

It is possible to choose the body force $F_x(r,x)$ such that only one radial acoustic mode, say $n = N$, is generated. This is done by taking

$$F_x(r,x) = y_{mN}(r)F(x) \tag{50}$$

so that $\widetilde{F}(r,k) = y_{mN}(r)\,\widetilde{F}(k)$. On substitution into (49), by the orthogonality property of the eigenfunctions, all F_n $(n = 1,2,\ldots)$ are zero except F_N. This gives

$$p(r,\phi,x,t) = \begin{cases} \dfrac{2\pi^2 k_N^+ \widetilde{F}(k_N^+) y_{mN}(r) \mathrm{e}^{\mathrm{i}(k_N^+ x + m\phi - \Omega t)}}{\Omega M + (1-M)k_N^+}, & x > 0 \\ \dfrac{-2\pi^2 k_N^- \widetilde{F}(k_N^-) y_{mN}(r) \mathrm{e}^{\mathrm{i}(k_N^- x + m\phi - \Omega t)}}{\Omega M + (1-M)k_N^-}, & x < 0, \end{cases} \tag{51}$$

where $\Omega^2 > (1-M^2)\lambda_{mn}^2$ for the mode to be a propagating mode. Formula (51) provides an exact analytical solution that is useful for validating results of direct numerical simulation of the acoustic modes generated by body forces in the flow.

Figure 11 shows the wavenumber of the four propagating acoustic modes for the case $M = 0.3$, $\overline{\Omega} = 0$, $m = 2$, $\Omega = 10.0$ and $\sigma = 0, 4$. Also shown (as filled circles) are the wavenumbers of the acoustic modes with a rigid-body swirl of $\overline{\Omega} = 0.5$. The effect of swirl is quite small in this case. The change in the eigenfunctions due to swirl is also quite small.

5. Discussion

For ducted inviscid compressible swirling flows, the wave modes do not form a complete set. As a result, ambiguity arises when a standard normal mode analysis is used to determine the intrinsic wave modes of the flow. Previous workers, using

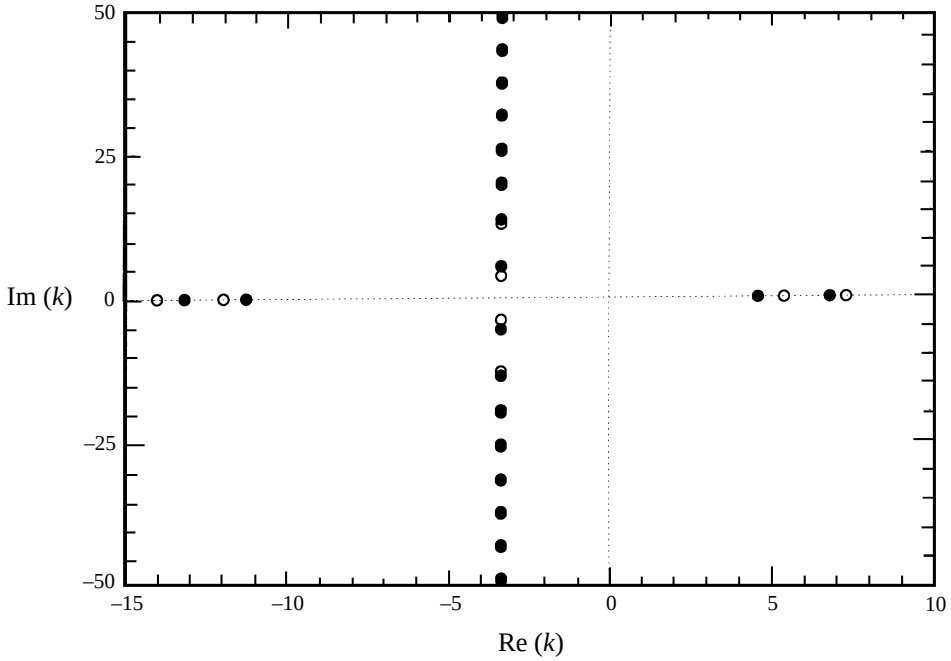

FIGURE 11. The magnified k-plane showing the effect of swirl on the acoustic modes: o, modes without rigid-body swirl; •, modes with rigid-body swirl.

such an approach, found a continuum of purely convected modes. We have shown by using the initial value approach that these modes are spurious. They are not the correct analytic continuation of the physical solution.

For a swirling flow inside an annulus, there are two families of waves. They are the acoustic modes and the rotational modes (assuming there are no unstable shear waves). In this work, we have investigated numerically these wave modes associated with simple model mean flows. For a non-simple mean flow with a general distribution of axial and azimuthal velocity components $\overline{u}(r)$ and $\overline{w}(r)$, the determination of the waves generated by a given body force distribution is not straightforward. An alternative way to find the waves produced is to use time-domain direct numerical simulation. However, to implement such a simulation, it is necessary to ensure there is adequate numerical resolution. For this purpose, one must have an idea of the magnitude of the wavenumbers of the modes involved. For the rotational modes, one can define an averaged angular velocity of the flow $\overline{\Omega}$ and use (36) to obtain k_1 and k_2. As an estimate one may use (37) to find the range of wavenumbers of the rotational modes. For the acoustic modes, only the propagating modes need be considered. The wavenumber of a propagating mode must be real. From (48), in order that $k_n^{\pm}$ is real the radial mode number n must be limited to the largest integer $\overline{N}$ such that

$$\Omega^2 > (1 - M^2)\lambda_{m\overline{N}}^2.$$

Here M is an average Mach number of the flow. With $\overline{N}$ determined, the relevant wavenumbers can be estimated by equation (48).

In this paper, we have confined our investigation to the determination of the number of families of wave modes an axially uniform swirling ducted flow will support and some of their propagation characteristics. The scope of this study is limited. It does

not extend to many interesting areas of applications in turbomachinery noise. In a turbofan engine, because of the presence of many rows of rotors and stators, there are, invariably, significant changes in the swirl in the axial direction of the engine. There exists in the literature a body of works devoted to the phenomenon of wave mode reflection and trapping as a result of axial variation in swirl. For a detailed analysis and discussion of this aspect of swirling flow and noise, the readers are referred to the works of Topol, Holhubner & Mathews (1987) and Hanson (1993, 1994).

The authors wish to thank Philip Gliebe of the GE Aircraft Engines for his encouragement and enthusiastic support of this investigation. Funding for this work was provided by the GE Aircraft Engines as part of an Independent Research and Development Project.

REFERENCES

Atassi, H. M. & Gredzinski, J. 1989 Unsteady disturbances of streaming motions around bodies. *J. Fluid Mech.* **209**, 385–403.

Chandrasekhar, S. 1961 *Hydrodynamic and Hydromagnetic Stability*. Oxford University Press.

Eversman, W. 1991 Theoretical model for duct acoustic propagation and radiation. In *Aeroacoustics of Flight Vehicles: Theory and Practice. Volume 2: Noise Control* (ed. H. H. Hubbard), Chap. 13, pp. 101–164. *NASA RP*–1258.

Goldstein, M. E. 1978 Unsteady vortical and entropic distortions of potential flows round arbitrary obstacles. *J. Fluid Mech.* **89**, 433–468.

Golubev, V. V. & Atassi, H. M. 1995 Aerodynamic and acoustic response of a blade row in unsteady swirling flow. *First Joint CEAS/AIAA Aeroacoustics Conferecnce* (*16th AIAA Aeroacoustics Conference*) *Munich, Germany, Paper* 95-027, pp. 167–176.

Golubev, V. V. & Atassi, H. M. 1997 Acoustic-vorticity modes in an annular duct with mean vortical swirling flow. *AIAA Paper* 97-1695.

Greitzer, E. M. & Strand, T. 1978 Asymmetric swirling flows in turbomachine annuli. *Trans. ASME* **100**, 618–629.

Hanson, D. B. 1993 Mode trapping in coupled 2D cascades – acoustic and aerodynamic results. *AIAA Paper* 93-4417.

Hanson, D. B. 1994 Coupled 2-dimensional cascade theory for noise and unsteady aerodynamics of blade row interaction in turbofans. Vol. 1, theory development and parametric studies. *NASA Contr. Rep.* 4506.

Kerrebrock, J. L. 1974 Waves and wakes in turbomachine annuli with swirl. *AIAA Paper* 74-87.

Kerrebrock, J. L. 1977 Small disturbances in turomachine annuli with swirl. *AIAA J.* **15**, 794–803.

Ko, S. H. 1973 Theoretical prediction of sound attenuation in acoustically lined annular ducts in the presence of uniform flow and shear flow. *J. Acoust. Soc. Am.* **54**, 1592–1606.

Kousen, K. A. 1995 Eigenmode analysis of ducted flows with radially dependent axial and swirl components. *First Joint CEAS/AIAA Aeroacoustics Conference* (*16th AIAA Aeroacoustics Conference*) *Munich, Germany, Paper* 95-160, pp. 1085–1094.

Kousen, K. A. 1996 Pressure modes in ducted flows with swirl. *AIAA Paper* 96-1679.

Kovasznay, L. S. 1953 Turbulence in supersonic flow. *J. Aero. Sci.* **20**, 657–674.

Lin, C. C. 1967 *The Theory of Hydrodynamics Stability*. Cambridge University Press.

Mungar, P. & Plumblee, H. E. 1969 Propagation and attenuation of sound in a soft-walled annular duct containing a sheared flow. *SP* 207, *NASA,* pp. 305–327.

Nayfeh, A. H., Kaiser, J. E. & Telionis, D. P. 1975 Acoustics of aircraft engine-duct systems. *AIAA J.* **13**, 130–153.

Pridmore-Brown, D. C. 1958 Sound propagation in a fluid flowing through an attenuating duct. *J. Fluid Mech.* **4**, 393–406.

Rayleigh, Lord 1916 On the dynamics of revolving fluids. *Scientific Papers,* vol. 6, pp. 447–453. Cambridge University Press.

Salant, R. F. 1968 Symmetric normal modes in a uniformly rotating fluid. *J. Acoust. Soc Am.* **43**, 1302–1305.

Scott, M. R. & Watts, H. A. 1977 Computational solutions of linear two-point boundary value problems via orthonormalization. *SIAM J. Numer. Anal.* **14**, 40–70.

Shankar, P. N. 1972 sound propagation in duct shear layers. *J. Sound Vib.* **22**, 221–232.

Swinbanks, M. A. 1975 The sound field generated by a source distribution in a long duct carrying sheared flow. *J. Sound Vib.* **40**, 51–76.

Tam, C. K. W. 1975 Supersonic jet noise generated by large scale disturbances. *J. Sound Vib.* **38**, 51–79.

Tam, C. K. W. & Hu, F. Q. 1989*a* On the three families of instability waves of high-speed jets. *J. Fluid Mech.* **201**, 447–483.

Tam, C. K. W. & Hu, F. Q. 1989*b* The instability and acoustic wave modes of supersonic mixing layers inside a rectangular channel. *J. Fluid Mech.* **203**, 51–76.

Tam, C. K. W. & Morris, P. J. 1980 The radiation of sound by instability waves of a compressible plane turbulent shear layer. *J. Fluid Mech.* **98**, 349–381.

Tan, C. S. & Greitzer, E. M. 1986 Nonaxisymmetric compressible swirling flow in turbomachine annuli. *AIAA J.* **24**, 92–100.

Topol, D. A., Holhubner, S. C. & Mathews, D. C. 1987 A reflection mechanism for aft fan tone noise from turbofan engines. *AIAA Paper* 87-2699.

Tyler, J. M. & Sofrin, T. G. 1962 Axial flow compressor noise studies. *SAE Trans.* **70**, 309–332.

Unruh, J. F. & Eversman, W. 1972 The transmission of sound in an acoustically treated rectangular duct with boundary layer. *J. Sound Vib.* **25**, 371–382.

Wundrow, D. W. 1994 Small amplitude disturbances in turbomachine flows with swirl. *NASA CR* 195406.

Yousefian, V . 1975 Propagation of disturbances in compressor annuli with solid body rotation and throughflow. PhD thesis, Department of Aeronautics and Astronautics, Massachussetts Institute of Technology.

Yurkovich, R. N. 1976 Attenuation of acoustic modes in circular and annular ducts in the presence of sheared swirling flow. *AIAA Paper* 76-498.